

SCIENTIFIC REPORTS



OPEN

Multilayer Optimization for the Quantum Internet

Laszlo Gyongyosi^{1,2,3} & Sandor Imre²

We define a multilayer optimization method for the quantum Internet. Multilayer optimization integrates separate procedures for the optimization of the quantum layer and the classical layer of the quantum Internet. The multilayer optimization procedure defines advanced techniques for the optimization of the layers. The optimization of the quantum layer covers the minimization of total usage time of quantum memories in the quantum nodes, the maximization of the entanglement throughput over the entangled links, and the reduction of the number of entangled links between the arbitrary source and target quantum nodes. The objective of the optimization of the classical layer is the cost minimization of any auxiliary classical communications. The multilayer optimization framework provides a practically implementable tool for quantum network communications, or long-distance quantum communications.

Quantum Internet is a communication network with quantum nodes and quantum links^{1–16} that allows to the parties to perform efficient quantum communications^{17–19}. The aim of quantum Internet^{5,8} and quantum repeater networks^{1,17–23} is to distribute quantum entanglement between distant nodes through a chain of intermediate quantum repeater nodes^{24–33}. In the quantum Internet, the quantum nodes share entangled connections that formulate entangled links^{1–6}. The quantum nodes store the quantum states in their local quantum memory for path selection and path recovery purposes^{1–3,8,24–33}. Since setting several attributes must be optimized in parallel in an arbitrary quantum network, the optimization problem formulates a multi-objective procedure. Formally, multi-objective optimization covers the minimization of quantum memory usage time (storage time), the maximization of entanglement throughput (number of transmitted entangled states per second of a particular fidelity) of entangled links^{1–6}, and the reduction of the number of entangled links between a source and a target quantum node^{8,24–33}. However, the problem does not end here since a quantum repeater network can be approached on the quantum transmission (quantum layer) level and on the auxiliary classical communication (classical layer) level that is required for the dynamic functioning of the quantum layer. Therefore, the problem is not just a multi-objective optimization problem in the quantum layer but also a multilayer optimization issue that covers the development of both the quantum and classical layers of a quantum repeater network.

Here, we define a multilayer optimization method for quantum repeater networks. This covers both the quantum layer and the classical layer of a quantum repeater network.

By utilizing the tools of quantum Shannon theory^{1–7}, the optimization of the quantum layer includes minimizing the usage of quantum memories in the nodes to reduce the storage time of entangled states, the maximization of entanglement throughput of the entangled links, and also these conditions have to be satisfied for the shortest path between a given source node and target quantum node (i.e., a multi-objective optimization of the quantum layer).

The aim of classical-layer optimization is to curtail the cost of auxiliary classical communications, which is required for such optimization. The cost of the classical communication covers all communication costs required to achieve the optimal quantum network state including the classical communication steps for overall quantum storage time minimization, entanglement throughput maximization, and the selection of a shortest path.

The multilayer optimization employs advanced methods to solve the multi-objective optimization of the quantum layer. We define the structures of the quantum memory utilization graph and the entanglement throughput tree for the multi-objective optimization of the quantum layer of a quantum repeater network. The quantum memory utilization graph models the quantum memory usage for entanglement storage. The entanglement throughput tree shows the entanglement throughput of entangled links with respect to the number of transmittable entangled states at a particular fidelity. Using these advanced constructions, we also define a method for the

¹School of Electronics and Computer Science, University of Southampton, Southampton, SO17 1BJ, UK. ²Department of Networked Systems and Services, Budapest University of Technology and Economics, Budapest, H-1117, Hungary.

³MTA-BME Information Systems Research Group, Hungarian Academy of Sciences, Budapest, H-1051, Hungary. Correspondence and requests for materials should be addressed to L.G.Y. (email: l.gyongyosi@soton.ac.uk)

optimal assignment of entangled states in the repeater nodes. The input of the quantum layer optimization procedure is the quantum memory utilization graph, while the output of the method is a set of entanglement throughput trees. The output identifies the optimal states of the quantum network with respect to the multi-objective optimization function.

Classical-layer optimization focuses on the minimization of the total cost of classical communications by utilizing swarm intelligence^{34–38}. This also defines a multi-objective problem since the cost has to be reduced with respect to the classical communication cost required for the minimization of quantum memory usage, the classical cost of entanglement throughput maximization of entangled links, and for the selection of the shortest path in the quantum layer. Classical-layer optimization uses some fundamentals of bacteria foraging models^{26,30–35} and probabilistic multi-objective uncertainty characterization^{31,39,40,44–46}.

The optimization framework requires no changes in the physical layer, so the framework is directly implementable by the current physical devices^{1–6,17–19} and quantum networking elements^{8,24–33}. The method is useful in quantum networking environments with diverse physical attributes (different quantum memory characteristics, quantum error correction, physical quantum nodes attributes, and transmission capabilities of noisy quantum links).

The novel contributions of our paper are as follows:

- *We conceive a complex optimization framework for quantum networks. It integrates the development of the quantum and classical layers of quantum repeater networks.*
- *Quantum-layer optimization utilizes the attributes of physical-layer quantum transmissions, quantum memory usage, and entanglement distribution via the framework of quantum Shannon theory.*
- *Classical-layer optimization focuses on minimizing any auxiliary communications related to the quantum layer and optimization.*
- *Multilayer optimization is applicable by current physical devices and quantum networking elements providing a solution for the optimization of arbitrary quantum networking scenarios with diverse physical attributes and environments.*

This paper is organized as follows. In Section 2, the system model is proposed. In Section 3, the optimization procedure of the quantum layer of quantum repeater networks is defined. Section 4 studies the optimization of the classical layer. Section 5 provides a performance evaluation. Finally, Section 6 concludes the paper. Supplemental material is included in the Appendix.

System Model

Our model assumes that the quantum repeater network consists of a source and target node with intermediate repeater nodes and a quantum switcher node. A quantum switcher node S operates as follows. Node S is a quantum repeater node capable of switching between the entangled connections stored in its local quantum memory and a permit of applying entanglement swapping on the selected connections. While an i -th quantum repeater node establishes only the entangled connections with the neighbor quantum repeater nodes, a switcher node is equipped with an extended knowledge about the quantum network to select between the entangled links. A general repeater node is not allowed to perform any link selection, since it is assumed in the model that a quantum repeater node has only local knowledge about the network. A switcher node based on its network knowledge can also send entanglement swapping commands to the quantum repeater nodes to define new paths in the network.

Let N be a quantum network, $N = (V, \mathcal{S})$, where V is a set of nodes, \mathcal{S} is a set of entangled links. Without loss of generality, the level L_l of an entangled link $E(x, y)$ is defined as follows. For an L_l -level entangled link, the hop distance between quantum nodes x and y is^{1,11}

$$d(x, y)_{L_l} = 2^{l-1}, \quad (1)$$

with $d(x, y)_{L_l} - 1$ intermediate nodes between the nodes x and y . The probability that an L_l -level entangled link $E(x, y)$ exists between nodes x, y is $\Pr_{L_l}(E(x, y))$, which depends on the actual network.

The S quantum switcher is modeled as a quantum node with the following attributes and permissions:

- *knowledge about the physical attributes of distant quantum repeater nodes and the entangled connections of N (e.g., entanglement fidelity, quantum memory status, link noise, etc),*
- *internal quantum memory for the storage of entangled states,*
- *quantum functionality:*
 - *permission to set new entangled connections between its local quantum system and a selected quantum node of the quantum network,*
 - *permission to switch between the stored entangled states to construct new paths,*
- *classical functionality:*
 - *permission to command distant quantum nodes of N via classical links (to construct new entangled connections in the network, to perform entanglement swapping between the selected nodes, other).*

The network model is illustrated in Fig. 1. The example network in Fig. 1(a) consists of six quantum repeater nodes $R_i, i = 1, \dots, 6$, and a quantum switcher S that switches between the entangled connections using its local quantum memory. The switcher also can perform entanglement swapping in the network. The switcher node S

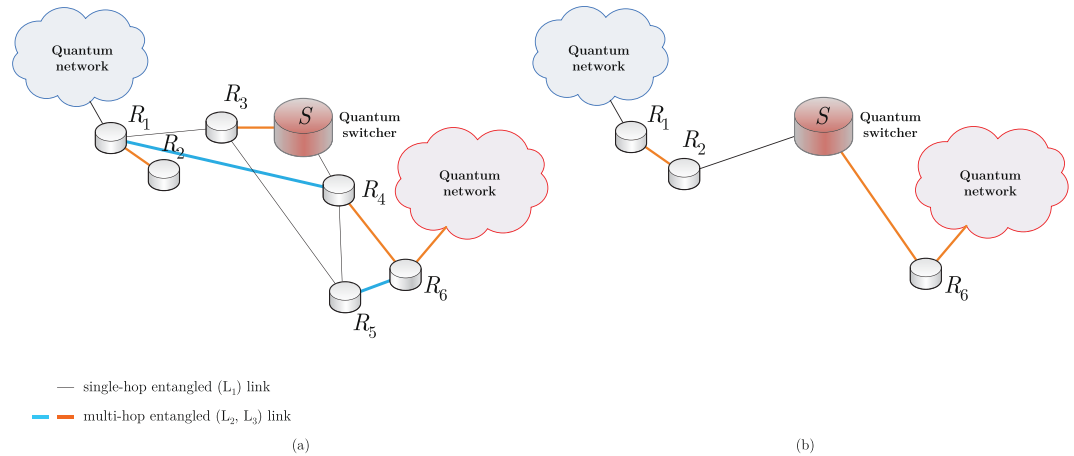


Figure 1. The network model with a quantum switcher S and quantum repeater nodes $R_i, i = 1, \dots, 6$. The L_1 , L_2 - and L_3 -level entangled links of N are depicted by gray, blue and orange, respectively (additional nodes are not shown). **(a)** For a current shortest path $\mathcal{P}_1 = \{R_1, R_3, S, R_4, R_6\}$, the active repeater nodes selected by S are R_3 and R_4 . **(b)** Node S switches the entangled connections in the local quantum memory from R_3 to R_2 and from R_4 to R_6 . The switching operation defines a new shortest path $\mathcal{P}_2 = \{R_1, R_2, S, R_6\}$.

has knowledge about the physical attributes (e.g., entanglement fidelity, quantum memory status, etc) of quantum repeater nodes to make a decision on a path. The knowledge about the repeater nodes can be transmitted over a classical link to the quantum switcher (classical links are not depicted). As it is depicted in Fig. 1(b), the switcher node has a permission to set new entangled connections via its local quantum state with a selected quantum node. The S switcher node decided to set a new entangled connection between its local quantum system and repeater node R_2 . A standard quantum repeater is not allowed to perform these operations (except with the direct neighbors in the entanglement distribution phase) without a dedicated command from the switcher.

Note, path \mathcal{P}_1 in Fig. 1(a) provides a shortest path at a particular network situation at an initial network time T_1 . Since the quantum network N evolves in time (quality of the entangled links, the status of the nodes, internal quantum memories, etc), at a given time T_2 , by utilizing the functions of the switcher node, the switcher node determined a new shortest path, \mathcal{P}_2 , as depicted in Fig. 1(b).

Quantum Memory Scheduling. In this section, we define a structure for scheduling quantum memory usage of the quantum nodes called the quantum memory utilization graph \mathcal{G}_m . This is a directed graph mapped from the network model, with several abstracted nodes and links.

Proposition 1 The \mathcal{G}_m quantum memory utilization graph is a directed graph with abstract nodes and links to schedule the quantum memory usage mapped from the quantum repeater network.

The \mathcal{G}_m graph of quantum memory utilization is constructed as follows. Assuming n quantum nodes (excluding the S switcher node) in the network, the graph contains n abstracted transmitter nodes and n abstracted receiver nodes with directed connections. Note if the quantum switcher S is modeled as the n -th node and $n_s = 1$, where n_s is the number of quantum switchers in N , the \mathcal{G}_m graph also can be constructed via $(n - 1)$ transmitter and $(n - 1)$ receiver quantum nodes. A given N with an arbitrary number of quantum switcher nodes defines a particular \mathcal{G}_m , therefore the \mathcal{G}_m graph is a combination of all other possible switcher modes. The \mathcal{G}_m graph contains directed edges between quantum node pairs $(V_x|V_y)$ and $(V_y|V_x)$ of a particular switcher mode $S_p, p = 1, \dots, N_s$, where N_s is the total number of switcher modes, depicted via nodes labeled as $(x|y)$ and $(y|x)$.

Let us assume that N has a single switcher node S , and it has two states, S_1 and S_2 . In both modes S_1 and S_2 , repeater node R_1 serves as a transmitter node for node R_2 .

In switcher mode S_1 , the shared entangled connection defines the following relations. Repeater node R_1 serves as a transmitter node for nodes R_3 and R_4 . Node R_3 serves as a transmitter node for nodes R_4 and R_5 . Node R_4 serves as a transmitter node for nodes R_5 and R_6 . Node R_5 serves as a transmitter node for node R_6 .

In switcher mode S_2 , the shared entangled connection defines the following relation. Repeater node R_2 serves as a transmitter node for node R_6 .

The \mathcal{G}_m graph of quantum memory utilization derived from the quantum network setting of Fig. 1. is illustrated in Fig. 2.

Entanglement Throughput Tree. In this section, we define the structure of the entanglement throughput tree, which aims to extract information from the quantum memory utilization graph. The entanglement throughput tree is also the output format of the multi-objective optimization procedure of the quantum layer.

Lemma 1 The \mathcal{G}_{et} entanglement throughput tree is a structure modeling the multi-objective optimization problem of quantum repeater networks. The tree structure is derived from the \mathcal{G}_m quantum memory utilization graph.

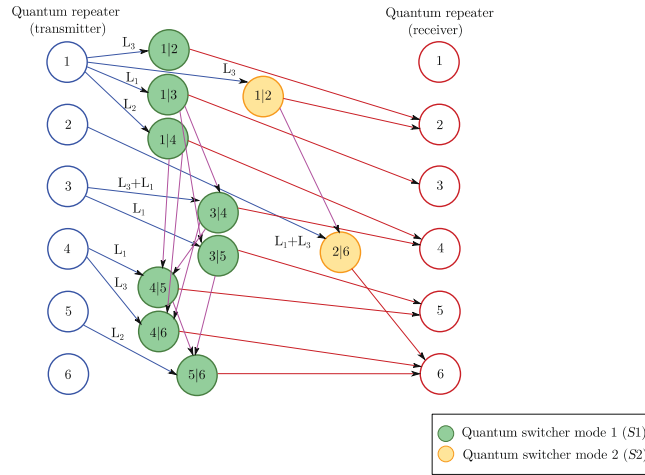


Figure 2. The \mathcal{G}_m graph of quantum memory utilization derived from the network setting in Fig. 1. The graph contains n abstracted transmitter nodes and n abstracted receiver nodes with directed entangled connections. An i -level entangled connect is depicted by L_i . The S quantum switcher has two states, S_1 and S_2 . The green circles represent quantum nodes operating on switcher mode S_1 . The yellow circles represent nodes operating on switcher mode S_2 .

Proof. As a given source node is selected, the next nodes are added to the path with a given probability.

Let us assume that \mathcal{G}_m is determined. Let us index the nodes by an ID identifier tag, $ID = \{A, B, \dots\}$, and let S_I be the set of unvisited neighbor nodes of a node I .

Let $B_F(E_{L_i}(I, J))$ refer to the entanglement throughput of a given L_i -level entangled link $E_{L_i}(I, J)$ between nodes (I, J) measured in the number of d -dimensional entangled states per second at a particular fidelity $F^{1,3,4}$.

Further, let J be a neighbor node of I with entangled connection $E_{L_i}(I, J)$ and with entanglement throughput $B_F(E_{L_i}(I, J))$.

A cost function, $\Omega(I, J)$, between nodes (I, J) is defined as

$$\Omega(I, J) = \frac{1}{C(E_{L_i}(I, J)) + \zeta_j}, \tag{1}$$

where $C(E_{L_i}(I, J))$ is the cost of entangled link $E_{L_i}(I, J)$ defined as

$$C(E_{L_i}(I, J)) = \frac{1}{B_F(E_{L_i}(I, J))}, \tag{3}$$

while ζ_j is the cost of quantum storage in node J .

Let $\lambda_{E_{L_i}(I, J)}$ be the entanglement utility coefficient of entangled link $E_{L_i}(I, J)$ between nodes I and J , initialized as $\lambda_{E_{L_i}(I, J)} \geq 0$. This amount is equivalent to the utility of the entangled link $E_{L_i}(I, J)$ that it has taken to arrive at the current node J from I .

At a given $B_F(E_{L_i}(I, J))$, the initial $\lambda_{E_{L_i}(I, J)}$ entanglement utility⁴ of link $E_{L_i}(I, J)$ is updated to $\lambda'_{E_{L_i}(I, J)}$ as

$$\begin{aligned} \lambda'_{E_{L_i}(I, J)} &= \left(\frac{1}{\lambda_{E_{L_i}(I, J)}} + B_F(E_{L_i}(I, J)) \right)^{-1} \\ &= \frac{\lambda_{E_{L_i}(I, J)}}{1 + B_F(E_{L_i}(I, J))\lambda_{E_{L_i}(I, J)}}. \end{aligned} \tag{4}$$

Using these cost functions, the $\Pr(I, J)$ probability that from node I a node J is selected is as follows:

$$\Pr(I, J) = \begin{cases} \frac{\left(\lambda'_{E_{L_i}(I, J)}\right)^{\omega^*} (\Omega(I, J))^\delta}{\sum_{\forall X \in S_I} \left(\lambda'_{E_{L_i}(I, X)}\right)^{\omega^*} (\Omega(I, X))^\delta}, & \text{if } J \in S_I, \\ 0, & \text{otherwise} \end{cases} \tag{5}$$

where ω^* and δ are weighting coefficients⁴.

Using (2), (3) and (5) for all node pairs, the \mathcal{M} method to build a random \mathcal{G}_{et} entanglement throughput tree using a \mathcal{G}_m graph is as follows^{36,37}.

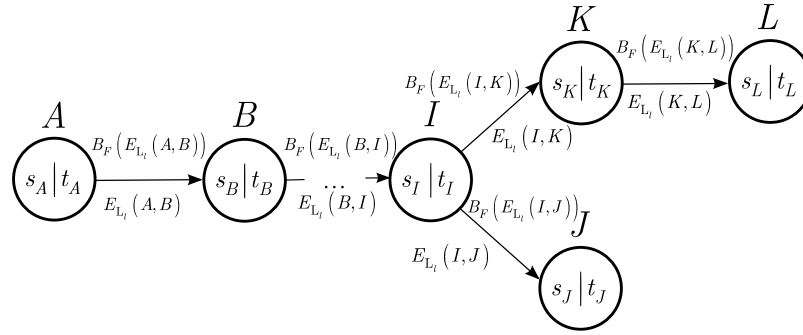


Figure 3. The structure of a \mathcal{G}_{et} entanglement throughput tree. A quantum node has an ID identifier tag, $ID = \{A, B, \dots, L\}$, and all incoming and outgoing entangled links are identified by the s_{ID} source neighbor node and the t_{ID} target neighbor node. Node A represents a source, while the destination nodes are J, K, L . The $B_F(E_{L_i}(x, y))$ entanglement throughput of all (x, y) node pairs are depicted above the directed lines; the link identifier $E_{L_i}(x, y)$ is depicted under the links.

Let S' refer to the set of already reached destination nodes, and let \mathcal{I} be the set of initial nodes, \mathcal{F}_I the set of feasible neighboring nodes to node I . Let \mathcal{D} be the set of destination nodes.

The method is given in Procedure 1.

Procedure 1. *Random Entanglement Throughput Tree Construction.*

- Step 1.** Initialize $\mathcal{G}_{et} = \emptyset, S' = \emptyset$. Select a node I of set \mathcal{I} and determine \mathcal{F}_I .
- Step 2.** If $\mathcal{F}_I = \emptyset$, then remove node I from \mathcal{I} , as $\mathcal{I} = \mathcal{I} - I$, otherwise compute probability $\Pr(I, J)$ via (5) for each node J of \mathcal{F}_I .
- Step 3.** Define uniformly distributed variable $x \in (0, 1]$. If $x > 0.5$, select that node J from \mathcal{F}_I that has large $\Pr(I, J)$. If $x \leq 0.5$, choose J randomly.
- Step 4.** Update sets \mathcal{G}_{et} and \mathcal{I} as $\mathcal{G}_{et} = \mathcal{G}_{et} \cup (I, J), \mathcal{I} = \mathcal{I} \cup J$. If node J is a destination node, $J \in \mathcal{D}$, then update set S' as $S' = S' \cup J$.
- Step 5.** Update $\lambda'_{E_{L_i}(I, J)}$ as $\lambda'_{E_{L_i}(I, J)} = (1 - \varphi) \lambda'_{E_{L_i}(I, J)} + \varphi \lambda_{E_{L_i}(I, J)}$, where φ is an evolution parameter, $\varphi \in [0, 1]$, and $\lambda_{E_{L_i}(I, J)}$ is the initial value of entanglement utility. Merge nodes of \mathcal{G}_{et} that duplicate entangled connections, and check the reachability of the nodes of \mathcal{D} .
- Step 6.** Repeat steps 2–5 until $\mathcal{I} \neq \emptyset$ or $S' \neq \emptyset$. Remove unused entangled links from \mathcal{G}_{et} and output \mathcal{G}_{et} .

The proof is concluded here. ■

The structure of a \mathcal{G}_{et} entanglement throughput tree is illustrated in Fig. 3.

Entanglement Assignment Cycle. In this section, we propose a solution for an optimal assignment (scheduling) of stored entanglement called the entanglement assignment cycle, $\alpha_{\mathcal{G}_{et}}$. The goal of $\alpha_{\mathcal{G}_{et}}$ is to achieve a minimal overall storage time $t_s^*(\mathcal{G}_{et})$ at a given \mathcal{G}_{et} entanglement throughput tree.

Lemma 2 *An entanglement assignment cycle can be determined by a weighted graph coloring method.*

Proof. To determine the minimal overall storage time for a \mathcal{G}_{et} entanglement throughput tree, the $\mathcal{C}_{\mathcal{G}_{et}}$ conflict graph of that \mathcal{G}_{et} is constructed first. In the $\mathcal{C}_{\mathcal{G}_{et}}$ graph, each vertex corresponds to a directed link of \mathcal{G}_{et} (an entangled connection). An edge exists between two vertices of $\mathcal{C}_{\mathcal{G}_{et}}$, if only the vertices (entangled connections) have a conflict. A conflict occurs if two (stored) entangled connects are associated to the same physical link. The problem is therefore to associate each link of \mathcal{G}_{et} a $\alpha_{\mathcal{G}_{et}}$ storage schedule (optimal assignment of stored entanglement), which includes the list of time slots when a given link can transmit the stored entangled states such that $\alpha_{\mathcal{G}_{et}}$ total number of time units is minimized. Therefore, our goal is to determine what entangled connects of the given \mathcal{G}_{et} should be scheduled in which time unit, such that the total storage time is minimal in $\alpha_{\mathcal{G}_{et}}$.

Let $\tau_{n,t} \in \{0, 1\}$ be an indicator variable, defined as

$$\tau_{n,t} = \begin{cases} 1, & \text{if } n \text{ is associated at } t \\ 0, & \text{otherwise} \end{cases} \tag{6}$$

For a periodic scheduling,

$$\tau_{n,t} = \tau_{n,t+iT} \quad (7)$$

where T is a period and i is a constant.

For an entangled connection n , let us define $\wedge(n)$ as the set of entangled connects n' that are scheduled in the same time unit t , but the physical link can transmit only n or n' . As follows, for any $n' \in \wedge(n)$,

$$\tau_{n,t} + \tau_{n',t} \leq 1. \quad (8)$$

As it can be concluded, this problem is analogous to the coloring of the conflict graph $\mathcal{C}_{\mathcal{G}_{et}}$.

Then, let us assume that each entangled connection (entangled link) has a weight $w(n)$, which is defined as

$$w(n) = \begin{cases} 1, & \text{if } F_i = F_{\max} \\ \left\lfloor \frac{F_{\max}}{F_i} \right\rfloor, & \text{if } F_i < F_{\max} \end{cases}, \quad (9)$$

where F_i is the fidelity of entangled connection i and F_{\max} is the largest fidelity available. As follows, for a lower-fidelity entangled connection, the transmission of a given amount of information requires more time units.

As the weights are determined, the problem is analogous to a weighted graph coloring of the conflict graph $\mathcal{C}_{\mathcal{G}_{et}}$, which is the assignment of at least $w(n)$ distinct colors to each entangled connection n such that no two entangled connections sharing the same color interfere with each other on the physical link. For this purpose, a simple distributed weighted coloring algorithm⁴⁶ can be straightforwardly applied.

The method for the $\mathcal{W}(\mathcal{C}_{\mathcal{G}_{et}})$ weighted coloring of conflict graph $\mathcal{C}_{\mathcal{G}_{et}}$ is summarized in Procedure 2.

Procedure 2. *Weighted Coloring of a Conflict Graph.*

Step 1. Determine conflict graph $\mathcal{C}_{\mathcal{G}_{et}}$ of \mathcal{G}_{et} , and compute weights $w(n)$ for all n . Assign weight $w(n)$ to vertex $n \in \mathcal{C}_{\mathcal{G}_{et}}$.

Step 2. Construct a new conflict graph $\mathcal{C}'_{\mathcal{G}_{et}}$ from $\mathcal{C}_{\mathcal{G}_{et}}$: for each vertex n with weight $w(n)$, create $w(n)$ vertices, $\{n_1, \dots, n_{w(n)}\}$, and add to $\mathcal{C}'_{\mathcal{G}_{et}}$.

Step 3. Add to $\mathcal{C}'_{\mathcal{G}_{et}}$ the edges connecting n_a and n_b , where $1 \leq a < b \leq w(n)$.

Step 4. Add to $\mathcal{C}'_{\mathcal{G}_{et}}$ the edge between i_a and j_b only if there is an edge between entangled connects i and j in $\mathcal{C}_{\mathcal{G}_{et}}$. Apply the unweighted vertex coloring algorithm [10] on $\mathcal{C}'_{\mathcal{G}_{et}}$.

Step 5. Assign n all the colors that are used by n_k , for $1 \leq k \leq w(n)$ in graph $\mathcal{C}'_{\mathcal{G}_{et}}$.

Step 6. Output the $\mathcal{W}(\mathcal{C}_{\mathcal{G}_{et}})$ weighted coloring of conflict graph $\mathcal{C}_{\mathcal{G}_{et}}$.

After an entanglement assignment cycle has been determined by the weighted graph coloring method, in the next step the $\Delta(\mathcal{W}(\mathcal{C}_{\mathcal{G}_{et}}))$ time intervals between each time unit of a given cycle is computed. For this purpose, a linear programming method⁴⁴ can be applied. ■

Quantum-Layer Optimization

In this section, we define the multi-objective optimization for the quantum layer. The multi-objective function covers a parallel optimization of quantum memory usage and entanglement throughput for a shortest path.

Theorem 1 *At a given \mathcal{G}_m , the quantum layer of a quantum repeater network N can be optimized by a procedure \mathcal{P}_Q that achieves a parallel minimization of the quantum memory usage time t_s , the maximization of entanglement throughput B_F , and the minimization of the number $|\mathcal{P}|$ of entangled links between two arbitrary nodes.*

Proof. The aim of the procedure is to find an optimal entanglement throughput tree \mathcal{G}_{et}^* for which the $t_s(\mathcal{G}_{et}^*)$ over-all storage time is minimal, that is,

$$t_s(\mathcal{G}_{et}^*) = t_s^*(\mathcal{G}_{et}^*); \quad (10)$$

the $B_F(\mathcal{G}_{et}^*)$ entanglement throughput for all links is maximal,

$$B_F(\mathcal{G}_{et}^*) = B_F^*(\mathcal{G}_{et}^*); \quad (11)$$

and the $|\mathcal{P}(\mathcal{G}_{et}^*)|$ number of entangled links of a path is minimal, thus

$$|\mathcal{P}(\mathcal{G}_{et}^*)| = |\mathcal{P}^*(\mathcal{G}_{et}^*)|, \quad (12)$$

where \mathcal{P}^* is the shortest path.

The procedure is based on the fact that for a given \mathcal{G}_{et}^* with conflict graph $\mathcal{C}_{\mathcal{G}_{et}^*}$, from the knowledge of $\mathcal{W}(\mathcal{C}_{\mathcal{G}_{et}^*})$ weighted coloring of conflict graph $\mathcal{C}_{\mathcal{G}_{et}^*}$, $\Delta(\mathcal{W}(\mathcal{C}_{\mathcal{G}_{et}^*}))$ time intervals between each time unit of a given cycle, the required objective values of (10), (11), and (12) can be determined.

Let $\mathcal{S}_{\mathcal{G}_{et}}^*$ be the set of optimal \mathcal{G}_{et}^* entanglement throughput trees. Then the aim of the procedure is to determine $\mathcal{S}_{\mathcal{G}_{et}}^*$. The problem can be rewritten via a solution set X with decision variables⁴⁴

$$X = \{x_1, \dots, x_n\}, \tag{13}$$

where n is the number of all links in a given quantum memory utilization graph \mathcal{G}_m , and $x_i \in \{0, 1\}$ is defined as

$$x_i = \begin{cases} 1, & \text{if link } i \text{ of } \mathcal{G}_m \text{ is selected by } \mathcal{M} \\ 0, & \text{otherwise.} \end{cases} \tag{14}$$

Let $X_{\mathcal{G}_{et}^i}$ be a solution i from solution set $X_{\mathcal{G}_{et}}$. Let $X_{\mathcal{G}_{et}^j} \angle X_{\mathcal{G}_{et}^i}$ refer to solution $X_{\mathcal{G}_{et}^j}$ dominating solution $X_{\mathcal{G}_{et}^i}$, which is

$$X_{\mathcal{G}_{et}^j} \angle X_{\mathcal{G}_{et}^i} : \{t_s^*(\mathcal{G}_{et}^i) \leq t_s^*(\mathcal{G}_{et}^j), \\ B_F^*(\mathcal{G}_{et}^i) \geq B_F^*(\mathcal{G}_{et}^j), \\ |\mathcal{P}^*(\mathcal{G}_{et}^i)| \leq |\mathcal{P}^*(\mathcal{G}_{et}^j)|\}, \tag{15}$$

and for these relations, there is at least strict inequality⁴⁴. If $X_{\mathcal{G}_{et}^i}$ dominates all other possible solutions, then $X_{\mathcal{G}_{et}^i}$ is a set of nondominated solutions.

For each set X , let κ refer to the set that contains the best nondominated solutions that have been found at a particular iteration. If κ changes, then the entanglement utilities of the links are updated. If κ is stationary, then the elements of set κ are used to update the entanglement utilities. The former serves as an improvement in the exploration process whereas the latter aims to yield more information via the best solutions⁴⁴.

At a given graph \mathcal{G}_m of quantum memory utilization, the procedure \mathcal{P}_Q for the optimization of the quantum layer is defined as follows. The output of \mathcal{P}_Q is an optimal set $\mathcal{S}_{\mathcal{G}_{et}}^*$ of entanglement throughput trees that realize the conditions of the multi-objective optimization function. The steps of the quantum layer optimization are summarized in Algorithm 1.

Note if there are no nondominated solutions, then the values of the weighting coefficients ρ , ς , and Υ in Step 5 of Algorithm 1 can be selected according to the actual trade-off requirements.

The proof is therefore concluded here. ■

Algorithm 1. *Quantum Layer Optimization.*

Step 1. Set $\mathcal{S}_{\mathcal{G}_{et}}^* = \emptyset$, and for all entangled connects, initialize $\lambda'_{E_{L_l}(I,J)}$ as

$$\lambda'_{E_{L_l}(I,J)} = \lambda_{E_{L_l}(I,J)}.$$

Step 2. Determine X , and apply method \mathcal{M} for building an \mathcal{G}_{et} entanglement throughput tree as $\mathcal{M}(X) = \mathcal{G}_{et}^X$. For a given \mathcal{G}_{et}^X , determine the $\alpha_{\mathcal{G}_{et}}$ optimal assignment of stored entanglement, the t_s^* overall minimal storage time, the B_F^* maximal entanglement throughput, and the $|\mathcal{P}^*|$ minimal number of entangled links, where \mathcal{P}^* is a shortest path.

Step 3. If X is not dominated by any $X_{\mathcal{G}_{et}} \in \kappa$, that is, $X_{\mathcal{G}_{et}} \angle X$ for any $X_{\mathcal{G}_{et}}$, then update κ as

$$\kappa = \kappa \cup X - \{X_{\mathcal{G}_{et}} | X_{\mathcal{G}_{et}} \angle X\}.$$

Step 4. If κ has been updated to κ' , then update the entanglement utility as

$$\lambda'_{E_{L_l}(I,J)} = \lambda_{E_{L_l}(I,J)}$$

Step 5. If κ has not been updated, then for all $X_{\mathcal{G}_{et}} \in \kappa$ compute

$$\Pi = \rho t_s(\mathcal{G}_{et}^X) + \varsigma B_F^*(\mathcal{G}_{et}^X) + \Upsilon |\mathcal{P}^*(\mathcal{G}_{et}^X)|,$$

where $t_s(\mathcal{G}_{et}^X)$ is the storage time associated to tree \mathcal{G}_{et}^X , $B_F^*(\mathcal{G}_{et}^X)$ is the maximal entanglement throughput associated to tree \mathcal{G}_{et}^X , $|\mathcal{P}^*(\mathcal{G}_{et}^X)|$ is the number of entangled links of the $\mathcal{P}^*(\mathcal{G}_{et}^X)$ shortest path of \mathcal{G}_{et}^X , while ρ , ς , and Υ are weighting coefficients. For all entangled links of graph \mathcal{G}_m , update $\lambda'_{E_{L_l}(I,J)}$ as

$$\lambda'_{E_{L_l}(I,J)} = (1 - \Pr(I, J)) \lambda'_{E_{L_l}(I,J)} + \Pr(I, J) \Pi.$$

Step 6. Output optimal entanglement throughput tree set $\mathcal{S}_{\mathcal{G}_{et}}^*$.

Classical-Layer Optimization

In this section we characterize the classical layer optimization procedure.

Theorem 2 *The cost function of classical communications can be minimized by a procedure \mathcal{P}_C .*

Proof. Let

$$\begin{aligned} f_{t_s^*, B_F^*, |\mathcal{P}^*|}(\Theta_i) &= \left(\sum_{g=1}^{N_{t_s^*}} S_{t_s^*, g}(i) + c_{N_{t_s^*}}^L(i) \right) + \left(\sum_{g=1}^{N_{B_F^*}} S_{B_F^*, g}(i) + c_{N_{B_F^*}}^L(i) \right) \\ &\quad + \left(\sum_{g=1}^{N_{|\mathcal{P}^*|}} S_{|\mathcal{P}^*|, g}(i) + c_{N_{|\mathcal{P}^*|}}^L(i) \right) \end{aligned} \quad (16)$$

be the cost function of classical communication of the multilayer optimization procedure, where $\Theta_i \in \mathbb{R}^p$ is a p -dimensional real vector of an i -th system state of the quantum network, $N_{t_s^*}$, $N_{B_F^*}$, $N_{|\mathcal{P}^*|}$ are the number of nodes that require the determination of optimal t_s^* , B_F^* and $|\mathcal{P}^*|$, $S_{t_s^*, g}(i)$, $S_{B_F^*, g}(i)$, $S_{|\mathcal{P}^*|, g}(i)$ refer to the number of classical steps required to find t_s^* , B_F^* and $|\mathcal{P}^*|$ for a particular node g of network N , while $c_{N_{t_s^*}}^L(i)$, $c_{N_{B_F^*}}^L(i)$, and $c_{N_{|\mathcal{P}^*|}}^L(i)$ are the costs of classical link L used for the determination of t_s^* , B_F^* and $|\mathcal{P}^*|$ for a given g .

Then, let introduce indices for Θ_i as

$$\Theta_i(j, k, l), \quad (17)$$

where j is the index of a desired optimal system state, k is the index of an optimal system state reproduction step, l is the index of a non-optimal system state event³⁹.

Let assume that there is a set of S sub-states $\{\Theta_1, \dots, \Theta_S\}$ in the network, then the T total network state is evaluated as

$$T(j, k, l) = \{\Theta_i(j, k, l) | i = 1, \dots, S\}. \quad (18)$$

Let $f_{t_s^*, B_F^*, |\mathcal{P}^*|}(\Theta_i(j, k, l))$ be the cost function of classical communication at a given $\Theta_i(j, k, l)$. Then, if

$$f_{t_s^*, B_F^*, |\mathcal{P}^*|}(\Theta_i(j+1, k, l)) < f_{t_s^*, B_F^*, |\mathcal{P}^*|}(\Theta_i(j, k, l)), \quad (19)$$

then the system state evolves from j to $j+1$ as

$$\Theta_i(j+1, k, l) = \Theta_i(j, k, l) + c(i)u(j), \quad (20)$$

where $c(i)$ is the number of random system states, while $u(j)$ quantifies a unit cost of system change^{39,40}.

Therefore, for a set of S sub-states $\{\Theta_1, \dots, \Theta_S\}$ and current vector $\Theta \in \mathbb{R}^p$, the C_N total cost of classical communication is yielded as

$$C_N(\Theta, \Theta_i(j, k, l)) = \sum_{i=1}^S f_{t_s^*, B_F^*, |\mathcal{P}^*|}(\Theta_i(j, k, l)), \quad i = 1, \dots, S, \quad (21)$$

which can be rewritten³⁹ as

$$\begin{aligned} C_N(\Theta, T(j, k, l)) &= \sum_{i=1}^S \left(-Ae^{-R_A} \sum_{m=1}^p (\Theta^{(m)} - \Theta_i^{(m)})^2 \right) + \sum_{i=1}^S \left(\nu e^{-R_\nu} \sum_{m=1}^p (\Theta^{(m)} - \Theta_i^{(m)})^2 \right) \end{aligned} \quad (22)$$

where A is the distribution-entropy of a current system state, R_A is the information transmission rate of A , ν is the distribution-entropy of a system state, R_ν is the information transmission rate of ν , while $\Theta^{(m)}$ is the m -th element of a current network state vector Θ , and $\Theta_i^{(m)}$ is the m -th element of Θ_i .

Using $C_N(\Theta, T(j, k, l))$ (see (22)), an environment-dependent cost function C_e is defined as

$$C_e = C_N(\Theta, T(j, k, l)) e^{\left(M - f_{t_s^*, B_F^*, |\mathcal{P}^*|}(\Theta_i(j, k, l)) \right)}, \quad (23)$$

where M is a tuning parameter³⁹.

From (23), the F_{cost}^i cost function at a given $\Theta_i(j, k, l)$ is defined as

$$F_{cost}^i = f_{t_s^*, B_F^*, |\mathcal{P}^*|}(\Theta_i(j, k, l)) + C_e(\Theta_i(j, k, l)). \quad (24)$$

Using the proposed basic model, we define an optimization procedure \mathcal{P}_C of the classical-layer to achieve a $C_N(\Theta, T(j, k, l))$ minimized cost function. The method is summarized in Algorithm 2.

These results conclude the proof. ■

Algorithm 2. *Classical Layer Optimization.*

Step 1. For an i -th system state $\Theta_i(j, k, l)$ initialize cost function

$$f_{t_s^*, B_F^*, |\mathcal{P}^*|}(\Theta_i(j, k, l)) = f_{t_s^*, B_F^*, |\mathcal{P}^*|}(\Theta_i(j, k, l)) + C_N(\Theta_i(j, k, l), T(j, k, l)).$$

Define a random network state vector $\partial(i) \in \mathbb{R}^p$, where the $\partial_m(i)$ m -th element of $\partial(i)$ is a uniformly distributed number from the range of $[-1, 1]$.

Step 2. From $\Theta_i(j, k, l)$, define $\Theta_i(j+1, k, l)$ as

$$\Theta_i(j+1, k, l) = \Theta_i(j, k, l) + c(i) \frac{\partial(i)}{\sqrt{(\partial(i))^T \partial(i)}},$$

where $c(i)$ is the number of random system states.

Step 3. Using $f_{t_s^*, B_F^*, |\mathcal{P}^*|}(\Theta_i(j, k, l))$, determine $f_{t_s^*, B_F^*, |\mathcal{P}^*|}(\Theta_i(j+1, k, l))$ as

$f_{t_s^*, B_F^*, |\mathcal{P}^*|}(\Theta_i(j+1, k, l)) = f_{t_s^*, B_F^*, |\mathcal{P}^*|}(\Theta_i(j, k, l)) + C_N(\Theta_i(j+1, k, l), T(j+1, k, l))$. If

$$f_{t_s^*, B_F^*, |\mathcal{P}^*|}(\Theta_i(j+1, k, l)) < f_{t_s^*, B_F^*, |\mathcal{P}^*|}(\Theta_i(j, k, l)),$$

update $f_{t_s^*, B_F^*, |\mathcal{P}^*|}(\Theta_i(j, k, l))$ as

$$f_{t_s^*, B_F^*, |\mathcal{P}^*|}(\Theta_i(j, k, l)) = f_{t_s^*, B_F^*, |\mathcal{P}^*|}(\Theta_i(j+1, k, l)).$$

Update $\Theta_i(j+1, k, l)$ as

$$\Theta_i(j+1, k, l) = \Theta_i(j, k, l) + c(i) \frac{\partial(i)}{\sqrt{(\partial(i))^T \partial(i)}},$$

and compute $f_{t_s^*, B_F^*, |\mathcal{P}^*|}(\Theta_i(j+1, k, l))$.

Step 4. Increase i , $i = i + 1$. If $i < S$, apply steps 1-3 for the current network sub-state. If $j < n_G(\tilde{\Theta})$, where $n_G(\tilde{\Theta})$ is the total number of iteration steps on j to reach an optimal global state $G(\tilde{\Theta})$, then increase j , $j = j + 1$.

Step 5. For all i , determine

$$F_{cost}^i = \sum_{j=1}^{n_G(\tilde{\Theta})+1} f_{t_s^*, B_F^*, |\mathcal{P}^*|}(\Theta_i(j, k, l)) + C_e(\Theta_i(j, k, l)).$$

Remove system states for which $F_{cost}^i \geq \chi_C$, where χ_C is a threshold on F_{cost}^i to get the minimized cost F_{cost}^{\min} as

$$F_{cost}^{\min} = \sum_{i=1}^{S-\varphi} F_{cost}^i,$$

where φ is the total number of removed system states. For a given E_k and E_l expected values of k and l , if $k < E_k$ then increase k , $k = k + 1$, and if $l < E_l$ increase l , $l = l + 1$.

Large-Constrained Optimization. The optimization efficiency can be further improved for a large constrained network scenario. This step can be replayed by a different approach, which allows an optimization of the classical layer for an arbitrary constrained setting. The solution is based on the idea of system state merging.

Lemma 3 *The optimization of the classical-layer can be extended to a large-constrained optimization by state merging.*

Proof. An extended model of the classical-layer optimization is as follows.

Let $N_{t_s^*}$, $N_{B_F^*}$, $N_{|\mathcal{P}^*|}$ be the number of nodes that require the determination of optimal t_s^* , B_F^* and $|\mathcal{P}^*|$. Then, let J be the objective function³⁴, as

$$J = \min \sum_{t=1}^T (\alpha_{t_s^*}(t) + \alpha_{B_F^*}(t) + \alpha_{|\mathcal{P}^*|}(t)), \quad (25)$$

where

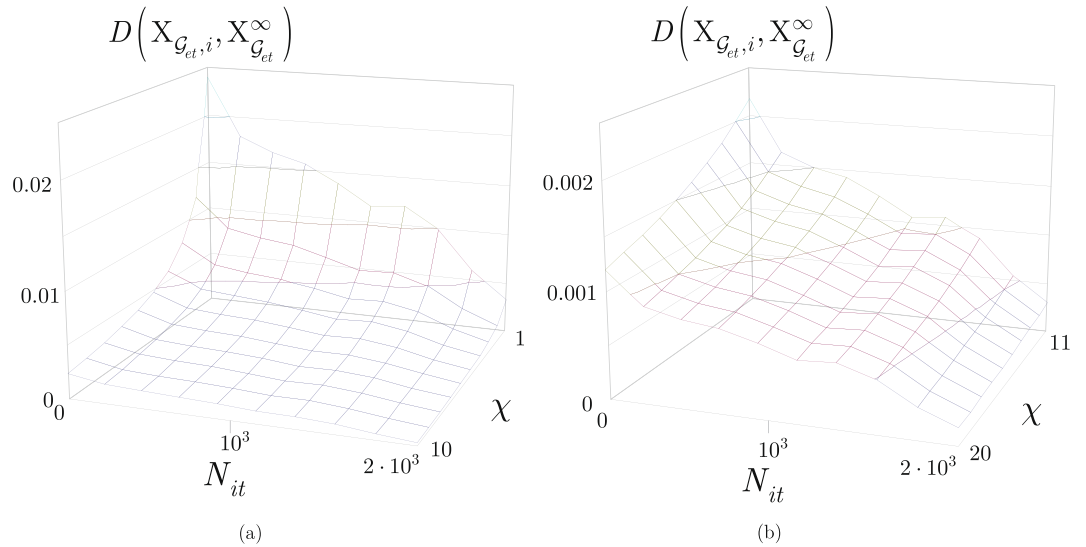


Figure 4. The $D(X_{G_{et},i}, X_{G_{et}}^\infty)$ distance in function of N_{it} and χ . **(a)** The values of $D(X_{G_{et},i}, X_{G_{et}}^\infty)$ for $0 < N_{it} \leq 2 \cdot 10^3$ and $1 \leq \chi \leq 10$. **(b)** The values of $D(X_{G_{et},i}, X_{G_{et}}^\infty)$ for $0 < N_{it} \leq 2 \cdot 10^3$ and $11 \leq \chi \leq 20$.

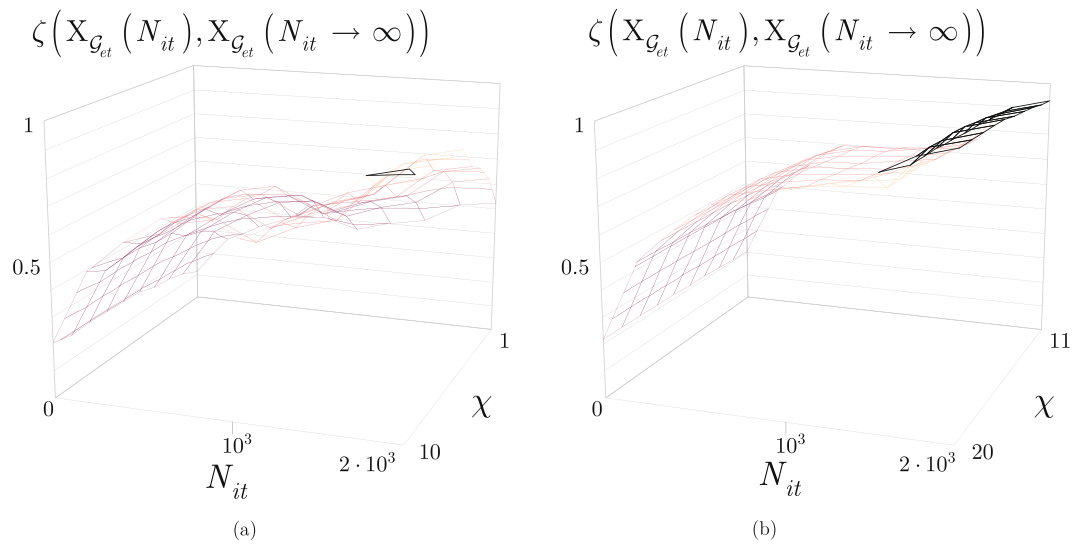


Figure 5. The ratio $\zeta(X_{G_{et}}(N_{it}), X_{G_{et}}(N_{it} \rightarrow \infty))$ in function of N_{it} and χ . **(a)** The values of $\zeta(X_{G_{et}}(N_{it}), X_{G_{et}}(N_{it} \rightarrow \infty))$ for $0 < N_{it} \leq 2 \cdot 10^3$ and $1 \leq \chi \leq 10$. **(b)** The values of $\zeta(X_{G_{et}}(N_{it}), X_{G_{et}}(N_{it} \rightarrow \infty))$ for $0 < N_{it} \leq 2 \cdot 10^3$ and $11 \leq \chi \leq 20$.

$$\alpha_{t_s^*}(t) = \sum_{g=1}^{N_{t_s^*}} S_{t_s^*,g}(t) + c_{N_{t_s^*}}^L(t), \tag{26}$$

$$\alpha_{B_F^*}(t) = \sum_{g=1}^{N_{B_F^*}} S_{B_F^*,g}(t) + c_{N_{B_F^*}}^L(t), \tag{27}$$

and

$$\alpha_{|P^*|}(t) = \sum_{g=1}^{N_{|P^*|}} S_{|P^*|,g}(t) + c_{N_{|P^*|}}^L(t), \tag{28}$$

where the coefficients $S_{t_s^*,g}(t), S_{B_F^*,g}(t), S_{|P^*|,g}(t)$ refer to the number of classical steps required to find t_s^*, B_F^* and $|P^*|$ at a particular network node g and time $t, t = 1, \dots, T$, while $c_{N_{t_s^*}}^L(t), c_{N_{B_F^*}}^L(t), c_{N_{|P^*|}}^L(t)$ are the costs of classical link

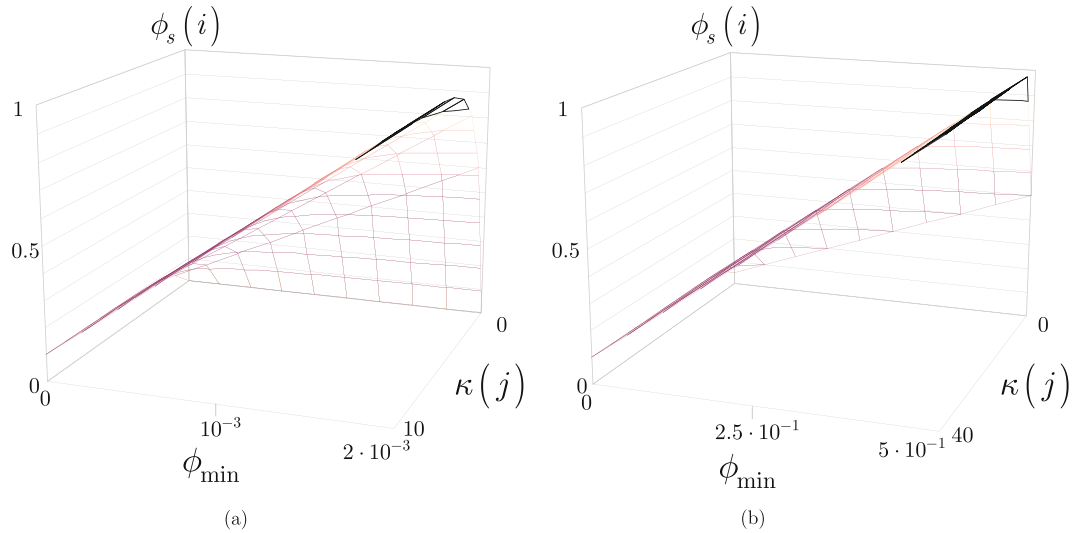


Figure 6. (a) The $\phi_s(i)$ step-size function for $\phi_{\min} \in [0, 2 \cdot 10^{-3}]$, $\phi_{\max} = 500\phi_{\min}$ and $\kappa(j) \in [0, 10]$. (b) The $\phi_s(i)$ step-size function for $\phi_{\min} \in [0, 5 \cdot 10^{-1}]$, $\phi_{\max} = 2\phi_{\min}$ and $\kappa(j) \in [0, 40]$.

L at a particular g and t . Let assume that $\Theta_a(j, k, l)$, $\Theta_b(j, k, l)$ and $\Theta_c(j, k, l)$ are some system states of the classical layer subject of state merging. From these sub-states, the $\Theta_M(j, k, l)$ merged system is defined as

$$\Theta_M(j, k, l) = \Theta_a(j, k, l) + \Phi(\Theta_b(j, k, l) - \Theta_c(j, k, l)), \tag{29}$$

where Φ is a merging factor, $\Phi \in [0, 1]$.

Using (29), an i -th system state $\Theta_i(j, k, l)$ is updated as

$$\Theta_i(j, k, l) = \left(\tilde{\Theta}_i^a(j, k, l), \tilde{\Theta}_i^b(j, k, l), \tilde{\Theta}_i^c(j, k, l) \right)^T, \tag{30}$$

where

$$\tilde{\Theta}_i^a(j, k, l) = \begin{cases} \Theta_i(j, k, l), & \text{if } x_a > u \\ \Theta_M(j, k, l), & \text{otherwise} \end{cases}, \tag{31}$$

$$\tilde{\Theta}_i^b(j, k, l) = \begin{cases} \Theta_i(j, k, l), & \text{if } x_b > u \\ \Theta^*(j, k, l), & \text{otherwise} \end{cases}, \tag{32}$$

and

$$\tilde{\Theta}_i^c(j, k, l) = \begin{cases} \Theta^*(j, k, l), & \text{if } x_c > u \\ \Theta_M(j, k, l), & \text{otherwise} \end{cases}, \tag{33}$$

where u is a uniform random number, x_a, x_b and x_c are random numbers, $x_a, x_b, x_c \in [0, 1]$, $\Theta^*(j, k, l)$ is a system state that minimizes the objective function J . Then for $Q \in (a, b, c)$, the objective function value $J(\tilde{\Theta}_i^Q(j, k, l))$ is compared with the objective function $J(\Theta_i(j, k, l))$ of $\Theta_i(j, k, l)$, and $\tilde{\Theta}_i^Q(j, k, l)$ is updated by the following rule:

$$\tilde{\Theta}_i^Q(j, k, l) = \begin{cases} \Theta_i(j, k, l), & \text{if } J(\tilde{\Theta}_i^Q(j, k, l)) < J(\Theta_i(j, k, l)) \\ \tilde{\Theta}_i^Q(j, k, l), & \text{otherwise.} \end{cases}, \tag{34}$$

The proof is concluded here. ■

Cost Uncertainty of Large-Scaled Optimization. The determination of the minimal cost function (25) is can be approached by an output variable $O_J = f(\psi_{in})$, where ψ_{in} is the set of input variables, and $f(\cdot)$ is a function that transfers the uncertainty from the independent input random variables ψ_{in} to the output variable O_J ³⁴. The output set O_J can be rewritten as

$$O_J = f(q, w_1, \dots, w_z), \tag{35}$$

where q is the set of certain variables, while w_i is an input variable under certainty with probability function $\delta_{f_{w_i}}$.

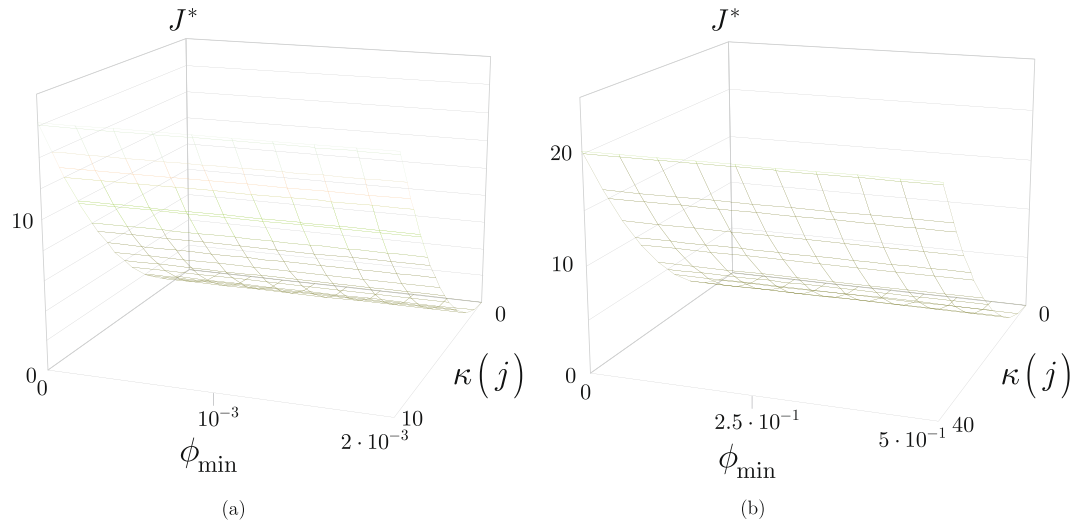


Figure 7. The J^* cost function values associated to the $\phi_s(i)$ step size function value, **(a)** $J_p = 1$ and $\omega = 1$, **(b)** $J_p = 1$ and $\omega = 100$.

Then, for a given variable w_p , two $pc(w_i)$ probability concentrations³⁴, $pc^{(1)}(w_i)$ and $pc^{(2)}(w_i)$ are defined as

$$pc^{(1)}(w_i) = (w_{i,1}, \zeta_{i,1}) \tag{36}$$

and

$$pc^{(2)}(w_i) = (w_{i,2}, \zeta_{i,2}), \tag{37}$$

where $w_{i,g}$, is the poth location of w_i ³⁴, $g = 1, 2$, while $\zeta_{i,g}$ is a weighting factor.

Therefore, at a given (i, g) parameterization, where $i = 1, \dots, z$ and $g = 1, 2$, O_j is expressed by variable $O_j^{(i,g)}$ as

$$O_j^{(i,g)} = f(q, w_{i,g}, \mu_{w_1}, \mu_{w_2}, \dots, \mu_{w_z}), \tag{38}$$

where μ_{w_i} is the mean of w_p , while $w_{i,1}$ and $w_{i,2}$ are the poth locations of w_i . Therefore, the problem is reduced to $2z$ deterministic equations³⁴, from which the mean and standard deviation of the output random variable $O_j^{(i,g)}$ can be computed.

Performance Evaluation

In this section we study the performance of the proposed quantum layer and classical layer optimization methods.

Quantum Layer Optimization. To study the convergence of the quantum layer optimization, we characterize the $D(\cdot)$ closeness function of the elements of the solution set from an optimal Pareto front, and the $\zeta(\cdot)$ ratio of optimal solutions in the solution set.

Let $X_{G_{et}^i} = \{t_s^*(G_{et}, i), B_F^*(G_{et}, i), |P^*(G_{et}, i)|\}$ be an i -th solution from the solution set $X_{G_{et}}(N_{it})$ found at a N_{it} finite number of iterations, and let $X_{G_{et}}^\infty = \{t_s^*(G_{et}, z), B_F^*(G_{et}, z), |P^*(G_{et}, z)|\}$ refer to a solution z from $X_{G_{et}}(N_{it} \rightarrow \infty)$ at $N_{it} \rightarrow \infty$. Then, let $D(X_{G_{et}^i}, X_{G_{et}}^\infty)$ be the distance on the Pareto front^{44–46} between $X_{G_{et}^i}$ and $X_{G_{et}}^\infty$, defined as

$$D(X_{G_{et}^i}, X_{G_{et}}^\infty) = \frac{1}{\chi}(A + B + C), \tag{39}$$

with $D(X_{G_{et}^i}, X_{G_{et}}^\infty) \in [0, 1]$, and where

$$A = \frac{|t_s^*(G_{et}, z) - t_s^*(G_{et}, i)|}{t_s^*(G_{et}, z)}, \tag{40}$$

$$B = \frac{|B_F^*(G_{et}, z) - B_F^*(G_{et}, i)|}{B_F^*(G_{et}, z)}, \tag{41}$$

and

$$C = \frac{||\mathcal{P}^*(\mathcal{G}_{et}, z)| - |\mathcal{P}^*(\mathcal{G}_{et}, i)||}{|\mathcal{P}^*(\mathcal{G}_{et}, z)|}, \tag{42}$$

while χ is a control parameter, $\chi > 0$.

Then, let $\zeta(X_{\mathcal{G}_{et}}(N_{it}), X_{\mathcal{G}_{et}}(N_{it} \rightarrow \infty))$ be a ratio of the solution sets $X_{\mathcal{G}_{et}}(N_{it})$ and $X_{\mathcal{G}_{et}}(N_{it} \rightarrow \infty)$ found at finite N_{it} and $N_{it} \rightarrow \infty$ as

$$\zeta(X_{\mathcal{G}_{et}}(N_{it}), X_{\mathcal{G}_{et}}(N_{it} \rightarrow \infty)) = \frac{card(X_{\mathcal{G}_{et}}(N_{it}) \wedge X_{\mathcal{G}_{et}}(N_{it} \rightarrow \infty))}{card(X_{\mathcal{G}_{et}}(N_{it}))}, \tag{43}$$

where $card(X_{\mathcal{G}_{et}}(N_{it}))$ is the cardinality of set $X_{\mathcal{G}_{et}}(N_{it})$, while $X_{\mathcal{G}_{et}}(N_{it}) \wedge X_{\mathcal{G}_{et}}(N_{it} \rightarrow \infty)$ is the intersection of solution sets $X_{\mathcal{G}_{et}}(N_{it})$ and $X_{\mathcal{G}_{et}}(N_{it} \rightarrow \infty)$ (solutions included by both solution sets). Note, since the χ control parameter in (39) determines the D distance from the optimal set, χ also affects the ratio of the solution sets (43). If the value of χ is high, the D distance in (39) is low, that results in a high cardinality of the intersection set in (43). If χ is low, the D distance in (39) is high, therefore the cardinality of the intersection set is small.

The quantity of (39) for various N_{it} and χ are depicted in Fig. 4. From the results it can be concluded that as N_{it} increases, the $D(X_{\mathcal{G}_{et}^i}, X_{\mathcal{G}_{et}}^\infty)$ distance significantly decreases, while the speed of convergence is controllable by χ . It also can be verified that the χ control parameter has a significant impact on $D(X_{\mathcal{G}_{et}^i}, X_{\mathcal{G}_{et}}^\infty)$, and the $D(X_{\mathcal{G}_{et}^i}, X_{\mathcal{G}_{et}}^\infty)$ distance can be made arbitrarily small via a moderate value for N_{it} .

In Fig. 5, the quantity of (43) is illustrated for different values of N_{it} . As N_{it} increases the $\zeta(X_{\mathcal{G}_{et}}(N_{it}), X_{\mathcal{G}_{et}}(N_{it} \rightarrow \infty))$ ratio increases significantly, while the χ control parameter has a moderate effect on the ratio of (43). The ratio exceeds 0.5 at $N_{it} \approx 0.5 \cdot 10^3$, and can be increased to arbitrarily high via a moderate increment in N_{it} .

The performance of the quantum layer optimization method is therefore approachable via the distance function (39) and ratio (43). The analysis revealed that at moderate N_{it} values, the precision of the optimization method can be arbitrary high via the selection of the χ control parameter. It also has been concluded, that a high ratio of the solutions at a finite and moderate N_{it} , are identical to the solutions at the limit case of $N_{it} \rightarrow \infty$.

Classical Layer Optimization. Let $\phi_s(i)$ be the step-size function defined for an i -th state as

$$\phi_s(i) = \phi_{\max} - \Delta(\phi) \cdot \exp\left(\frac{-f(i,j,k,l)}{j}\right), \tag{44}$$

where

$$\Delta(\phi) = (\phi_{\max} - \phi_{\min}), \tag{45}$$

where ϕ_{\min} and ϕ_{\max} are some lower and upper bounds, $\phi_s(i) \in [\phi_{\min}, \phi_{\max}]$, while $f(i, j, k, l)$ is defined as

$$f(i, j, k, l) = \omega \frac{J^*}{J_p}, \tag{46}$$

where ω is a constant (restriction factor⁴¹⁻⁴³), J^* is the minimal cost function (for J , see (25)) at a particular parameter setting (i, j, k, l) , J_p is the minimal cost function associated to the population.

Then, at an iteration number j let $\kappa(j)$ be a ratio as

$$\kappa(j) = \frac{f(i,j,k,l)}{j}. \tag{47}$$

The step-size (44) in function of ϕ_{\min} and $\kappa(j)$ is depicted in Fig. 6.

From (44) and (46), the optimal cost function J^* at a particular setting of (i, j, k, l) is yielded as

$$J^* = -\frac{\ln\left(\frac{\phi_{\max} - \phi_s(i)}{\Delta(\phi)}\right)j}{\omega} J_p. \tag{48}$$

Then, let

$$\kappa(j) = x, \tag{49}$$

from which the iteration number can be rewritten as

$$j = \frac{f(i,j,k,l)}{x}, \tag{50}$$

and also fix $f(i, j, k, l)$ as

$$f(i, j, k, l) = x^2. \tag{51}$$

Then, from (49) and (51), J^* can be evaluated at a given x in function J_p and ω , as

$$J^* = \frac{x^2 J_p}{\omega}. \tag{52}$$

From (50) and (51), the function in (48) can be rewritten as

$$\begin{aligned} J^* &= -\frac{\ln\left(\frac{\phi_{\max} - \phi_s(i)}{\Delta(\phi)}\right) f(i, j, k, l)}{\omega x} J_p \\ &= -\frac{\ln\left(\frac{\phi_{\max} - \phi_s(i)}{\Delta(\phi)}\right) x}{\omega} J_p, \end{aligned} \quad (53)$$

therefore the cost function J^* at a particular (49) and (51) can also be evaluated in function of the step size (44).

The J^* cost function values associated to the $\phi_s(i)$ step size function values of Fig. 6 at $J_p = 1$ and $J_p = 1$ and $\omega = 100$ are depicted in Fig. 7.

The analysis is therefore revealed that for any $\phi_s(i)$, the cost function J^* increases with the $\kappa(j)$ ratio, and the values of J^* are tunable via the control parameter ω for arbitrary J_p and $\kappa(j)$ values. The proposed classical layer optimization model is therefore flexible, and allows a dynamics adaption for diverse environmental settings. As future work, our aim is to provide a transmission analysis and comparisons with other schemes.

Conclusions

Here we conceived a multilayer optimization method for the quantum Internet. Multilayer optimization defines separate procedures for the optimization of the quantum layer and the classical layer. Quantum-layer optimization defines a multi-objective function by minimizing the total usage of quantum memories in the quantum nodes, maximizing the entanglement throughput over all entangled links, and reducing the number of entangled links between the arbitrary source and target quantum nodes. We defined the structure of the quantum memory utilization graph and entanglement throughput tree. The classical-layer optimization utilizes the fundamentals of swarm intelligence for the minimization of the cost function. Since the proposed multilayer optimization method has no physical layer requirements, it can serve as a useful tool for quantum network communications and future quantum Internet.

References

1. Van Meter, R. *Quantum Networking*. ISBN 1118648927, 9781118648926 (John Wiley and Sons Ltd, 2014).
2. Gyongyosi, L., Imre, S. & Nguyen, H. V. A Survey on Quantum Channel Capacities. *IEEE Communications Surveys and Tutorials* **99**, 1, <https://doi.org/10.1109/COMST.2017.2786748> (2018).
3. Pirandola, S. Capacities of repeater-assisted quantum communications. *arXiv:1601.00966* (2016).
4. Gyongyosi, L. & Imre, S. Entanglement-Gradient Routing for Quantum Networks, *Sci. Rep., Nature*, <https://doi.org/10.1038/s41598-017-14394-w> (2017).
5. Lloyd, S. *et al.* Infrastructure for the quantum Internet. *ACM SIGCOMM Computer Communication Review* **34**, 9–20 (2004).
6. Imre, S. & Gyongyosi, L. *Advanced Quantum Communications - An Engineering Approach*. (Wiley-IEEE Press, New Jersey, 2013).
7. Gyongyosi, L. & Imre, S. Entanglement Availability Differentiation Service for the Quantum Internet, *Sci. Rep., Nature*, <https://doi.org/10.1038/s41598-018-28801-3> (2018).
8. Kimble, H. J. The quantum Internet. *Nature* **453**, 1023–1030 (2008).
9. Muralidharan, S., Kim, J., Lutkenhaus, N., Lukin, M. D. & Jiang, L. Ultrafast and Fault-Tolerant Quantum Communication across Long Distances. *Phys. Rev. Lett.* **112**, 250501 (2014).
10. Lloyd, S. The Universe as Quantum Computer. *A Computable Universe: Understanding and exploring Nature as computation*, Zenil, H. ed., *arXiv:1312.4455v1* (World Scientific, Singapore, 2013).
11. Gyongyosi, L. and Imre, S. Decentralized Base-Graph Routing for the Quantum Internet. *Phys. Rev. A*, American Physical Society, <https://doi.org/10.1103/PhysRevA.98.022310> (2018).
12. Caleffi, M. End-to-End Entanglement Rate: Toward a Quantum Route Metric, 2017 IEEE Globecom, <https://doi.org/10.1109/GLOCOMW.2017.8269080>, (2018).
13. Van Meter, R., Satoh, T., Ladd, T.D., Munro, W.J. & Nemoto, K. Path selection for quantum repeater networks. *Networking Science*, **3**, Issue 1–4, 82–95, (2013).
14. Caleffi, M. Optimal Routing for Quantum Networks, *IEEE Access*, **5**, <https://doi.org/10.1109/ACCESS.2017.2763325> (2017).
15. Caleffi, M., Cacciapuoti, A.S. and Bianchi, G. Quantum Internet: from Communication to Distributed Computing, *arXiv:1805.04360* (2018).
16. Castelvecchi, D. The quantum internet has arrived, *Nature*, News and Comment, <https://www.nature.com/articles/d41586-018-01835-3> (2018).
17. Pirandola, S., Laurenza, R., Ottaviani, C. & Banchi, L. Fundamental limits of repeaterless quantum communications. *Nature Communications* **15043**, <https://doi.org/10.1038/ncomms15043> (2017).
18. Pirandola, S. *et al.* Theory of channel simulation and bounds for private communication. *Quantum Sci. Technol.* **3**, 035009 (2018).
19. Laurenza, R. & Pirandola, S. General bounds for sender-receiver capacities in multipoint quantum communications. *Phys. Rev. A* **96**, 032318 (2017).
20. Vedral, V., Plenio, M. B., Rippin, M. A. & Knight, P. L. Quantifying Entanglement. *Phys. Rev. Lett.* **78**, 2275–2279 (1997).
21. Vedral, V. The role of relative entropy in quantum information theory. *Rev. Mod. Phys.* **74**, 197–234 (2002).
22. Petz, D. *Quantum Information Theory and Quantum Statistics* (Springer-Verlag, Heidelberg, Hiv: 6, 2008).
23. Bacsardi, L. On the Way to Quantum-Based Satellite Communication. *IEEE Comm. Mag.* **51**(08), 50–55 (2013).
24. Yuan, Z. *et al.* *Nature* **454**, 1098–1101 (2008).
25. Kok, P. *et al.* Linear optical quantum computing with photonic qubits. *Rev. Mod. Phys.* **79**, 135–174 (2007).
26. Biamonte, J. *et al.* Quantum Machine Learning. *Nature* **549**, 195–202 (2017).
27. Lloyd, S., Mohseni, M. & Rebentrost, P. Quantum algorithms for supervised and unsupervised machine learning. *arXiv:1307.0411* (2013).
28. Lloyd, S., Mohseni, M. & Rebentrost, P. Quantum principal component analysis. *Nature Physics* **10**, 631 (2014).
29. Lloyd, S. Capacity of the noisy quantum channel. *Physical Rev. A* **55**, 1613–1622 (1997).
30. Gisin, N. & Thew, R. Quantum Communication. *Nature Photon.* **1**, 165–171 (2007).
31. Shor, P. W. Scheme for reducing decoherence in quantum computer memory. *Phys. Rev. A* **52**, R2493–R2496 (1995).
32. Chou, C. *et al.* Functional quantum nodes for entanglement distribution over scalable quantum networks. *Science* **316**(5829), 1316–1320 (2007).
33. Sheng, Y. B. & Zhou, L. Distributed secure quantum machine learning. *Science Bulletin* **62**, 1025–2019 (2017).

34. Motevasel, M. & Bazyari, S. Probabilistic Energy Management of micro-grids with respect to Economic and Environmental Criteria. *Science Journal (CSJ)* **36**(3), Special Issue, ISSN: 1300–1949 (2015).
35. Farooq, M. & Di Caro, G. A. Routing protocols for next generation networks inspired by collective behaviors of insect societies: an overview. *Swarm Intelligence, Natural Computing Series*, pages 101–160 (2008).
36. Di Caro, F. D. G. & Gambardella, L. M. Swarm intelligence for routing in mobile ad hoc networks. *IEEE Swarm Intelligence Symposium*, pages 76–83 (2005).
37. Saleem, G. A. D. C. M. & Farooq, M. Swarm intelligence based routing protocol for wireless sensor networks: survey and future directions. *Information Sciences* **181**(20), 4597–4624 (2011).
38. Neumann, F. & Witt, C. Bioinspired computation in combinatorial optimization algorithms and their computational complexity. *Natural Computing Series* (2010).
39. Rani, B. S. & Kumar, C. A. A Comprehensive Review on Bacteria Foraging Optimization Technique, *Multi-objective Swarm Intelligence*, Theoretical Advances and Applications, Studies in Computational Intelligence, Volume 592 (Springer, 2015).
40. Liu, Y. & Passino, K. M. Biomimicry of Social Foraging Bacteria for Distributed Optimization: Models, Principles, and Emergent Behaviors. *Journal of Optimization Theory and Applications* **115**(3), 603–628 (2002).
41. Zhang, Y., Zhou, W. & Yi, J. A Novel Adaptive Chaotic Bacterial Foraging Optimization Algorithm, *2016 International Conference on Computational Modeling, Simulation and Applied Mathematics* (2016).
42. Niu, B., Fan, Y., Xiao, H. & Bing, X. Bacterial foraging based approaches to portfolio optimization with liquidity risk. *Neruocomputing* **98**, 90–100 (2012).
43. Li, M. S., Ji, T. Y., Tang, W. J., Wu, Q. H. & Saunders, J. R. Bacterial foraging algorithm with varying population. *Biosystems* **100**(3), 185–197 (2010).
44. Jie, Y. & Kamal, A. E. Multi-Objective Multicast Routing Optimization in Cognitive Radio Networks, *IEEE Wireless Communications and Networking Conference* (IEEE WCNC, 2014).
45. Pinto, D. & Baran, B. Solving multiobjective multicast routing problem with a new ant colony optimization approach. *Proceedings of ACM, International IFIP/ACM Latin American Conference on Networking* (2005).
46. Wang, W. *et al.* Efficient interference-aware TDMA link scheduling for static wireless networks. *Proceedings of ACM, International Conference on Mobile Computing and Networking* (2006).

Acknowledgements

This work was partially supported by the National Research Development and Innovation Office of Hungary (Project No. 2017-1.2.1-NKP-2017-00001), by the Hungarian Scientific Research Fund - OTKA K-112125 and in part by the BME Artificial Intelligence FIKP grant of EMMI (BME FIKP-MI/SC).

Author Contributions

L.G.Y. designed the protocol and wrote the manuscript. L.G.Y. and S.I. analyzed the results. All authors reviewed the manuscript.

Additional Information

Supplementary information accompanies this paper at <https://doi.org/10.1038/s41598-018-30957-x>.

Competing Interests: The authors declare no competing interests.

Publisher's note: Springer Nature remains neutral with regard to jurisdictional claims in published maps and institutional affiliations.



Open Access This article is licensed under a Creative Commons Attribution 4.0 International License, which permits use, sharing, adaptation, distribution and reproduction in any medium or format, as long as you give appropriate credit to the original author(s) and the source, provide a link to the Creative Commons license, and indicate if changes were made. The images or other third party material in this article are included in the article's Creative Commons license, unless indicated otherwise in a credit line to the material. If material is not included in the article's Creative Commons license and your intended use is not permitted by statutory regulation or exceeds the permitted use, you will need to obtain permission directly from the copyright holder. To view a copy of this license, visit <http://creativecommons.org/licenses/by/4.0/>.

© The Author(s) 2018